Engineering of Graphene Layer Orientation to Attain High Rate Capability and Anisotropic Properties in Li-Ion Battery Electrodes

*Amartya Mukhopadhyay, Fei Guo, Anton Tokranov, Xingcheng Xiao, Robert H. Hurt, and Brian W. Sheldon**

Novel carbon films with different graphene layer orientations are investigated as electrode materials for Li-ion batteries. It is demonstrated that engineering the crystallographic orientation with graphene layers oriented perpendicular to the surface substantially alters stress evolution during Li insertion. With this crystallographic orientation the intercalating/de-intercalating Li-ions also have direct access to the graphene interlayer spaces, resulting in higher capacity at faster electrochemical cycling, compared to carbon films with graphene layers parallel to the film surface. Electrodes with perpendicular alignment are prepared by supramolecular synthesis using either spin coating or bar coating of chromonic liquid crystal precursors into precursor organic films followed by in situ carbonization. These materials are compared with in situ stress measurements during lithiation/delithiation cycles, and the bar-coated films exhibit a highly anisotropic stress which is consistent with long-range alignment of the graphene layers. In contrast, the in-plane stresses in the spin-coated films are isotropic, which is consistent with the presence of randomly oriented domains (still with graphene layers oriented perpendicular to the surface). Overall, the use of thin film graphitic materials with controlled crystallographic orientations provides a valuable platform for investigating the impact of graphene structure on the properties of Li-ion battery electrode materials.

1. Introduction

Lithium ion batteries possess very high energy storage density and are presently used in a variety of small appliances and for nearly all portable electronic devices.[1–3] To utilize this energy density for larger scale applications such as electric vehicles or back-up storage for wind and solar energy, significant increases in the power density are needed.[1,4–6] This requires electrode materials with faster charging/discharging capabilities, which is currently a major focus of research directed towards alternative energy sources. The relatively slow solid state diffusion of Li-ions in intercalation electrode materials[1,2,7–12] often limits Li-ion battery capabilities, and higher power can be attained by developing novel electrode materials or devising strategies for increasing the overall transport rate of Li ions in the presently used materials. Recently, Ceder and co-workers proposed designs for improving Li-ion diffusivity in cathode materials via microstructural and crystallographic engineering.[4,5] The graphite particles that are widely used as anodes have graphitic domains with a variety of orientations that are not easily controlled. With this in mind, the thin film approaches we present here are specifically designed to permit controlled investigation of Li transport and other relevant properties.

Graphitic carbon intercalates Li-ions reversibly in interlayer spaces [(0002) planes], a property that has led to the widespread use of these materials as anodes in Li-ion batteries. The Li diffusivity is reported to be relatively fast parallel to the graphene layers ($\approx 10^{-6}$ cm^2 s^{-1}).[7–10] However, the graphite particles used for most batteries consist of grains with a variety of orientations, where some diffusion must also occur in the c-direction. These rates can be ≈4–6 orders of magnitude lower[7] and thus generally limit the overall intercalation kinetics. It is widely believed that Li-ion diffusion across a perfect graphene basal plane is essentially impossible, and that diffusion in this direction must thus occur through defects or along graphite grain/domain boundaries. Faster Li transport can thus be achieved by engineering the crystallographic orientation and defect structures of graphite electrodes.

One approach is to provide easier Li access to the interlayer spaces by orienting the material with the graphene edges in direct contact with the electrolyte. In this report, we demonstrate this concept experimentally via investigation of the

Dr. A. Mukhopadhyay
High Temperature and Energy Materials Laboratory
Department of Metallurgical Engineering and Materials Science
Indian Institute of Technology (IIT) Bombay
Powai, Mumbai 400076, India
Dr. A. Mukhopadhyay, F. Guo, A. Tokranov, Prof. R. H. Hurt, Prof. B. W. Sheldon
School of Engineering, Brown University
Providence, RI 02912, USA
E-mail: Brian_Sheldon@brown.edu
Dr. X. Xiao
General Motors Global R&D Center
Warren, MI 48090, USA

DOI: 10.1002/adfm.201201128

electrochemical behavior of graphenic carbon thin films with vertically aligned graphene layer arrays (VAGLAs). These materials are then compared directly with graphitic carbon films that have more conventional graphene layer orientations, with surfaces that are terminated primarily by basal planes.

2. Results and Discussion

2.1. Crystallographic Orientations of the Carbon Films and Electrode Architecture

We recently developed the VAGLA films using chromonic liquid crystal precursors,[13,14] as outlined in the schematic representation and TEM images in **Figure 1**a. In another recent work,[15] we used chemical vapor deposition (CVD) to produce carbon films of similar thickness and substrate/interlayer/film design, but with graphene planes (0002) parallel to the film surface (see also Figure 1b). Figure 1 presents schematic representations of the active carbon thin film/interlayer/substrate designs for both types of films (VAGLA and CVD C). The carbon films (≈200-nm thick) were grown on 250-µm-thick quartz substrates, with a Ni layer (≈200-nm thick) acting as the current collector[15] and a very thin (≈20 nm) Ti adhesion layer between the quartz substrate and the Ni layer. The Ni current collector promotes graphitization,[16] during the formation of both the CVD C[15] and VAGLA films.[13] Transmission electron microscopy (TEM) shows lattice fringes corresponding to (0002) graphite planes (Figure 1), which confirm the presence of well-ordered graphitic material. Due to the crystallographic orientation of the VAGLA films (graphene layers perpendicular to substrate), conventional XRD on these materials does not provide information about the (0002) graphene layer spacing. TEM (cross-section) observations and XRD measurements (glancing angle) on the CVD films confirm the presence of well-ordered graphene layers parallel to the substrate/current collector.[15] Unlike the CVD C films, the well-ordered TEM lattice fringes were not observed uniformly across the VAGLA films, even though both materials use the same Ni current collector and 1000 °C processing temperatures (heat treatment for VAGLA and deposition for CVD C). The poor graphitization in the VAGLA films is consistent with the nature of the molecular precursor,[13] which aligns over long length scales but does not polymerize to fill 2D space effectively, and contains significant heteroatom functionality (H, N, S). The result is a system that has a high degree of long-range orientational order among its constituent graphene layers set by the liquid crystal intermediate, but a low degree of atomic perfection within each layer due to high defect density and limited lateral dimension of the disk-like molecular precursor.[13] These two "modes" of order (orientational, atomic in-plane) are a unique feature of the VAGLA material, and lead to an unusual combination of anisotropic stress and voltage profiles described below. Nevertheless, the most important distinction is that the graphene planes are oriented perpendicular to the substrate in the VAGLA films (Figure 1a and ref. [13]), which is further confirmed by additional experimental results that are reported below.

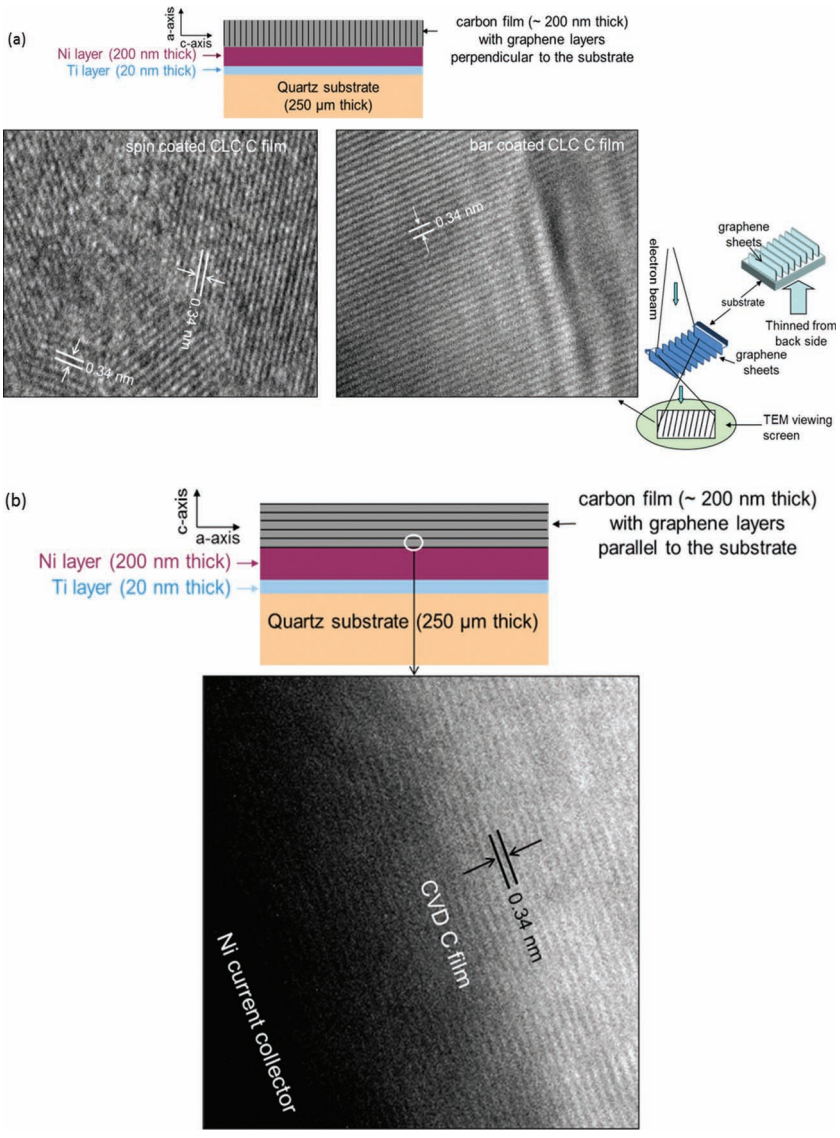

Figure 1. Schematic representation of film/substrate architecture and lattice fringe TEM images for a) VAGLA films, fabricated by spin coating or bar coating of disk-like organic precursors, as observed under planar view mode (schematic of the sample preparation and viewing mode presented by the side); b) CVD C film, as observed in cross-sectional mode.

The VAGLA films for the present investigation were prepared by both spin-coating and bar-coating with the chromonic liquid crystal precursors. For the spin-coated films, TEM reveals graphene layers that are perpendicular to the surface as noted

above, with grains/domains that are randomly oriented with respect to the substrate. This should lead to isotropic in-plane properties for these films. In the bar-coated films the vertically aligned graphene layers were oriented along the same lateral (in-plane) direction at all the locations. This orientation was also confirmed with lattice fringe images, and should lead to strongly anisotropic in-plane properties.

2.2. Electrochemical Cycling and In Situ Stress Measurement

For the CVD C films, we recently reported near theoretical reversible Li capacities (≈370 mAh g^{-1}).[15] Complementary information about the mechanical response of these graphitic films during Li intercalation and de-intercalation was also obtained with in situ in-plane stress measurements, using a multi-beam optical stress sensor (MOSS).[15,17,18] In the current investigation, similar variations in the potential and stress responses confirm the different structures of the spin-coated and bar-coated VAGLA films. Results for both of these materials during the first 10 electrochemical cycles at a constant rate of C/10 are shown in **Figure 2**. The voltage plateaus that are normally observed in fully graphitized carbons are not apparent here, which is consistent with the high atomic-scale defect density in VAGLA.

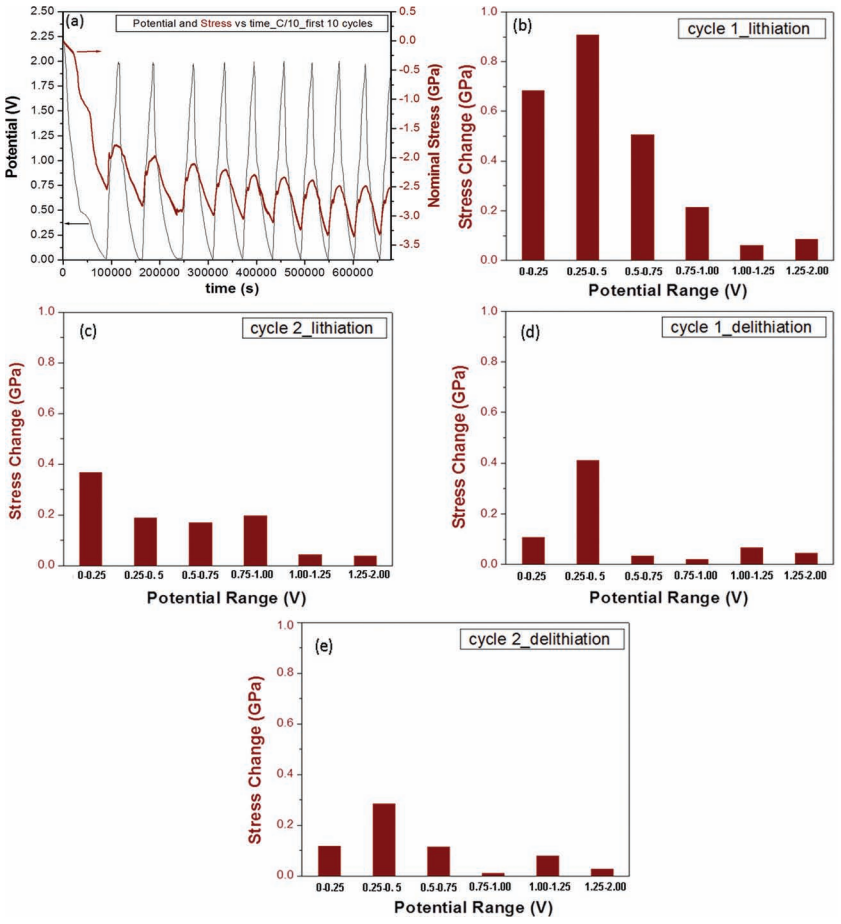

Figure 2. a) Electrochemical (potential vs time) and stress (determined in situ using MOSS) behavior for the first 10 cycles at a constant current rate of C/10 and b) stress developments at the different potential ranges during lithiation and delithiation half-cycles for the first two cycles of spin coated VAGLA film, cycled at C/10.

In the VAGLA films, there is some notable irreversible capacity loss and large irreversible stress (≈−2 GPa) during the first cycle. In subsequent cycles both the irreversible capacity and the irreversible stress decrease significantly. Similar variations of irreversible capacity and stress with cycling were also observed for the CVD C films. However, the first cycle irreversible stress was almost an order of magnitude less for the CVD C films.[15] Recently, we analyzed and attributed most of the irreversible stress development in the CVD materials to SEI layer formation, along with some contribution from solvated Li-ion co-intercalation.[19] Based on this interpretation, comparisons between the two types of films suggest that the stresses related to the irreversible processes of SEI layer formation (and solvated ion co-intercalation) are much more severe for the VAGLA films. It is well known that non-graphitic carbons can lead to irreversible capacity,[20,21] which does not have a major contribution in the better-graphitized CVD films.[15] However, it is important to note that the first cycle irreversible capacity for the two materials is comparable, with Coulombic efficiency (CE) in the VAGLA films (≈0.31) that is only marginally lower than the CVD C films (≈0.34). Thus, while there could be irreversible capacity in the VAGLA that is associated with disordered carbon there is not direct evidence for these effects in the CE values. A more likely contribution to the larger first cycle stress-thickness in the VAGLA films is that stresses associated with SEI layer formation are more pronounced on the graphene edge planes.[22] In the VAGLA films, these graphene edges directly face the electrolyte, compared to the basal planes which face the electrolyte in the CVD C films. It has also been reported that SEI layers on the edge planes contain a higher fraction of inorganic compounds, compared to SEI formed on the basal planes.[22] The substantially higher irreversible stress-thickness contribution in the VAGLA material is thus consistent with more substantial solvated ion co-intercalation and/or with more high-modulus inorganic SEI formation (e.g., Li_2CO_3 and LiF phases).

To understand the electrochemical behavior of the different carbon materials investigated here, it is also important to look more closely at stress evolution during the different voltage ranges (see Figure 2b,e). Since actual lithium intercalation for graphitic carbon takes place below ≈0.25 V against Li,[21–23] any compressive stress development at higher potentials can be related to the irreversible processes of SEI formation, solvated ion co-intercalation, and insertion in non-graphitic carbon. Against this backdrop, a large fraction of the stress development

in the first lithiation half cycle occurs at higher potentials, starting at ≈1 V. This value corresponds to solvated ions and the onset of SEI layer formation.[22,24–26] Stresses at these higher voltages are significantly reduced in the subsequent lithiation half cycles, where the majority of the stress then occurs reversibly below 0.25 V (compare Figure 2b,c). During the first delithiation half cycle, there is very little stress reversal recorded above 0.5 V (compare Figure 2b,c with Figure 2d,e), which also implies that the higher voltage stresses are largely irreversible. Very similar behavior was also documented with the CVD C films,[26] where we have attributed the irreversible stress to SEI formation and solvated-ion co-intercalation.[26,27] In these comparisons, the most notable differences in the VAGLA films are the much larger stress and the higher stress reversal in the 0.25–0.5 V potential range. All of these effects are consistent with SEI and solvated ion related differences that are associated with the carbon film crystallographic orientations. Stresses that are associated with SEI formation are expected to play an important role in the structural integrity of the SEI, in ways that should directly influence the cycle life of rechargeable batteries. Thus, the large difference in the SEI-related stress response due to the carbon orientation is an important finding. A better understanding of the stress contributions and relevant mechanisms warrants more detailed investigations with our model thin film electrode configurations and in situ stress measurements.

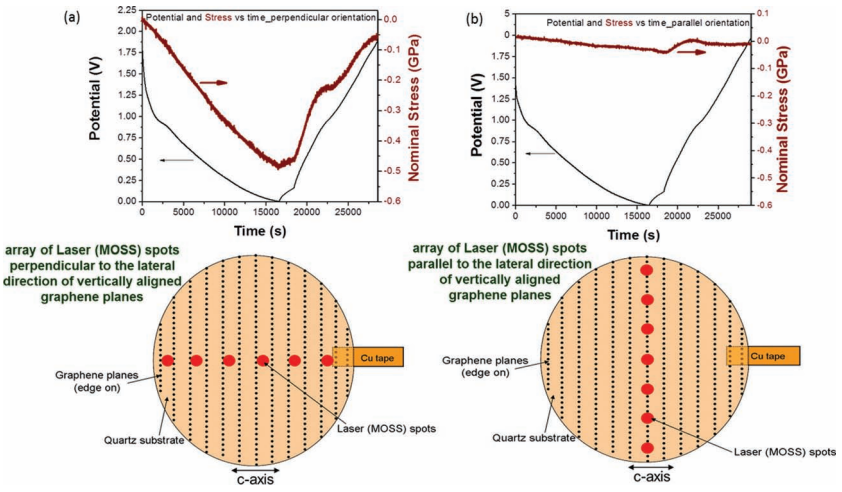

Figure 3. Variation of Potential and Stress (determined in situ using MOSS), along with schematic representations (as viewed from back side of substrate) of the alignment of the laser (MOSS) spot array with respect to the lateral direction of the vertically aligned graphene planes for the bar coated VAGLA films when the MOSS spots array is a) perpendicular to the lateral direction of graphene planes and b) parallel to the lateral direction of graphene planes. The electrochemical cycling rate used was C/5.

Similar to the CVD C films,[15,19] the capacity and concomitant stress generation for the spin coated VAGLA films was much more reversible after ≈15 cycles, with the CE exceeding ≈0.9. This implies that the SEI layer was stable, and after this point several experiments were performed at different electrochemical cycling rates (from C/20 to 10C). A maximum Li-deintercalation capacity of ≈404 mAh g^{-1} was recorded at the slowest rate, which is slightly higher than the theoretical capacity of graphitic carbon (≈372 mAh g^{-1}). Since the VAGLA films contain more atomic-scale disorder, this higher capacity is not unreasonable.[20,21] During Li-ion intercalation at C/20 the maximum compressive stress, measured parallel to the substrate/current collector (in-plane thin film stress), was ≈ –0.8 GPa.

2.3. Anisotropy in Stress Development for Bar-Coated VAGLA Films

Because the bar-coated VAGLA films have aligned graphene layers oriented vertically with respect to the substrate, and are also aligned in-plane in the same lateral direction along the substrate (Figure 1a), it was possible to measure the stress anisotropy in these films directly. During these in situ measurements the laser was first aligned with the substrate with the array of spots oriented at right angle to the lateral orientation of the graphene layers. With this configuration significant stress development was observed during cycling as seen in **Figure 3**a. On the other hand, with the array of MOSS spots oriented parallel to the lateral orientation of the graphene layers, the stress during cycling was much smaller (Figure 3b).

During Li-intercalation/de-intercalation to/from the graphene interlayer spaces, it is well established that the lithiation induced strains are highly anisotropic (i.e., ≈10% along the graphitic c-axis and ≈1% along the graphitic a-axis[28,29]). The substrate constrains this dilation/contraction, resulting in stress development, and thus the measured stress anisotropy in the bar-coated films confirms orientation of these films (i.e., when the laser spots are aligned along the graphite c-axis the spot spacing changes due to the induced substrate curvature are much larger). The much smaller stress measured parallel to the graphene layers is consistent with the much smaller lithiation induced dilation along the a-axis of graphite.[15,28,29] The absolute stresses measured in both directions are significantly lower than predicted values for pure graphite (based on literature values for the elastic modulus and lithiation induced strains), likely reflecting atomic-scale disorder. This initial set of experiments clearly demonstrates that bar-coated films possess highly anisotropic properties that reflect long-range orientational order in their graphene layer structure, and that they are this type of carbon may be suitable for novel functional applications, including the development of composite electrode materials which can benefit from controlled anisotropy; for instance, architectures capable of strain accommodation in one direction.

As described in the previous section, the measured stresses in the spin-coated VAGLA films did not exhibit the anisotropy seen in the bar-coated films. The random grain structure of these films combined with the highly anisotropic properties of graphite makes it more difficult to compare the measured stresses in these materials with expected behavior based on literature values. However, since the magnitude of these stresses

is comparable to those seen in the bar-coated films, it appears that these stresses are lower than what one would expect for randomly oriented graphite grains (with the c-axis in the plane of the film). It should also be noted that the measured lithiation induced in-plane stresses for the CVD C films (with c-axis oriented out of the plane of the substrate) were also lower than those predicted for pure graphite.[15] Thus, in all of these materials there appear to be mechanisms which lower the effective in-plane stiffness of the carbon. Possible explanations include stress accommodation at grain boundaries and other effects from non-graphitic carbon. However, the comparisons between these materials clearly indicate that different crystallographic orientations in the CVD and different types of VAGLA films lead to significantly different stress evolution during Li insertion. Note also that the lower than expected in-plane stress for these films is potentially advantageous, since this should lead to longer cycle life by limiting electrode degradation.

2.4. Variation of Li-Capacity with Electrochemical Cycling Rate

The reversible capabilities of both the VAGLA and CVD C films at high rates are compared in **Figure 4**a, for electrochemical cycling from C/20 to 10C. For both materials the Li capacities and concomitantly the lithiation induced reversible stresses decreased as the cycling rates increased. There are some very significant differences between the two materials at the higher rates. For the CVD C material, very little variation with capacity is noted for the slower three rates (C/20, C/10 and C/5), and beyond these rates the capacity drops rapidly with very little lithium capacity recorded for the two fastest rates (5C and 10C). By contrast, for the VAGLA films the capacity drops steadily but less rapidly from C/5 onwards. Hence, significant capacity was still obtained films at the highest cycling rates. In recently reported work, Yang et al.[30] also obtained good capacities at higher electrochemical cycling rates using hollow carbon-sphere based electrodes which had nanochannels in the radial direction, facilitating easier access for the Li-ions.

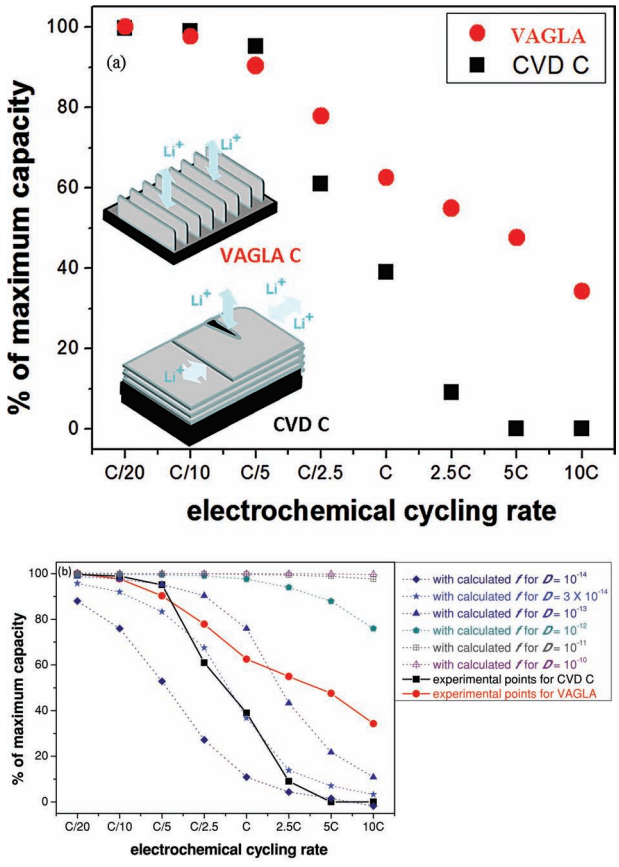

Figure 4. a) Variation of capacity (as percentage of maximum capacity) with electrochemical cycling rates (from C/20 to 10C) for the VAGLA and CVD C films; b) Fits corresponding to Equation (5), showing good fit for the CVD C film experimental results (against cycling rate) at D_{Li} between 10^{-13} and 10^{-14} cm^2 s^{-1}. This one parameter model does not exhibit a good fit to the experimental results for the VAGLA film at any D_{Li}.

The results in Figure 4a are indicative of kinetic limitations in both materials, while comparison shows that VAGLA and CVD materials behave differently. Li diffusion and electron conduction can both contribute to the observed rate dependence. It is well established that both species move faster along graphene layers (i.e., through the thickness of the VAGLA films). In comparison, Li ions have virtually no mobility through the perfect graphite basal plane.[7–10,31,32] Thus, in the CVD C films the Li-ions are almost certainly limited by diffusion through domain boundaries/defect sites on the basal planes, which has led to reports of lower Li diffusivity in this direction by ≈5 orders of magnitude,[7–10,31,32] and lower electrical conductivity by up to ≈2 orders of magnitude.[33,34] The relatively sharp decrease in capacity with increasing C rate for the CVD C is consistent with this relatively slow kinetics in the electrode material. In comparison, the substantially higher capacities in the VAGLA films at higher rates in Figure 4a are consistent with the expectation that there is faster transport of Li and/or electrons, because the vertical alignment of the graphene layers provides the intercalating Li-ions with direct access to the graphene interlayer spaces. Thus, based on the comparison in Figure 4a, greater capacity retention is possible for the VAGLA films at the higher cycling rates. In other words, electrode materials based on the VAGLA architecture (crystallographic orientation of the graphene layers) should allow development of batteries possessing higher rate capabilities, which is a significant result.[1,4–6]

The experiments reported here do not permit us to evaluate the ionic and electronic conductivities in the two materials, however, values reported in the literature[33,34] provide some basis for comparison. For example, the electrical conductivity along the a-axis is ≈2×10^4 S cm^{-1}, whereas that along the c-axis is ≈2×10^2 S cm^{-1}.[33,34] As noted above, this ≈2 orders of magnitude in electronic conductivity difference is much smaller than ≈5 orders of magnitude for diffusivity of Li ions along the two orientations.[7–10,31,32] Furthermore, assuming a Li diffusivity (D_{Li}) of ≈10^{-12} cm^2 s^{-1} along the c-axis,[7–10,31,32] the ionic conductivity of Li$^+$ (σ_{Li}) can be roughly estimated as be ≈4×10^{-12} S cm^{-1} using the Nerst–Einstein equation ($\sigma_{Li} = D_{Li}.F^2/RT$, where F is the Faraday's constant, R is the universal gas constant and T is temperature). Similarly, assuming a Li-ion diffusivity of ≈10^{-6} cm^2 s^{-1} along the a-axis (upper bound),[7–10,31,32] the Li-ion conductivity would be ≈4×10^{-6} S cm^{-1}. These values

are significantly lower than the electron conductivities cited above, which suggests that Li-ion conduction is more likely to be rate limiting. However, these comparisons do not provide definitive proof, and direct measurements on our materials are still needed.

To provide some additional comparisons between the thin film results in Figure 4a and reported data for Li transport in carbon electrodes, we also employ a simple diffusion analysis. This approach uses a phenomenological diffusivity, D, that does not attempt to address the relative contributions from ionic and electronic conductivity. This type of more rigorous treatment would require comparisons with more detailed electrochemical measurements, and is thus beyond the scope of the present paper. Furthermore, based on the above rough estimation, the relative contributions of electronic conductivity are expected to be significantly lower. The simpler Fick's law approach that we have employed is also consistent with other phenomenological modeling that is widely used.

To obtain an approximate estimate of the diffusivities that would correspond to our experimental results, we solve Fick's second law with a constant diffusivity, D:

$$\frac{\partial c}{\partial t} = D\frac{\partial^2 c}{\partial z^2} \tag{1a}$$

using appropriate initial and boundary conditions that are given by:

$$c(z,0) = c_o \quad at\ z = 0: \ \frac{\partial c}{\partial z} = 0 \quad at\ z = h: \quad \frac{\partial c}{\partial z} = \frac{j_S}{D} \tag{1b}$$

where j_S is the constant flux of Li that is determined by the fixed current density, $I = Fj_S$. The solution to Equation (1) is then given by[35]:

$$c(z,t) = c_o + \frac{j_S h}{D}\left[\theta + \frac{3z^2 - h^2}{6h^2} - \frac{2}{\pi^2}\sum_{n=1}^{\infty}\frac{(-1)^n}{n^2}\cos\left(\frac{n\pi z}{h}\right)\exp(-n^2\pi^2\theta)\right] \tag{2}$$

where $\theta = \frac{Dt}{h^2}$. For the CVD material, we consider Li insertion with an initial concentration of $c_o = 0$, and relatively small cell impedance outside of the electrode (i.e., Li transport to the surface is relatively fast). In this case the end of an insertion cycle occurs when the outer surface, $z = h$, reaches the concentration $c(h, t^*) = c^*_{eq}$. For graphitic carbon, this is given by:

$$c^*_{eq} = \frac{0.166}{V^*_m} \tag{3}$$

where the constant 0.166 corresponds to a cutoff voltage of 0 V (i.e., fully lithiated LiC_6), and V^*_m is the LiC_6 volume per mole of carbon. Inserting this surface condition into Equation (2) then gives:

$$1 = \rho\left[\theta^* + \frac{1}{3} - \frac{2}{\pi^2}\sum_{n-1}^{\infty}\frac{\exp(-n^2\pi^2\theta^*)}{n^2}\right] \tag{4}$$

where $\rho = j_s h / D c^*_{eq}$. The fractional capacity of the electrode during this insertion step is then given by:

$$f^* = \frac{\int_0^h c(z,t^*)dz}{h\,c^*_{eq}} = \rho\,\theta^* = 1 - \rho\left[\theta^* + \frac{1}{3} - \frac{2}{\pi^2}\sum_{n-1}^{\infty}\frac{\exp(-n^2\pi^2\theta^*)}{n^2}\right] \tag{5}$$

This general result, along with the experimental data points, is plotted in Figure 4b. This comparison shows that Equation (5) provides a good fit to the experimentally determined fractional capacity data for the CVD carbon films. The best fit show here corresponds to $D \approx 3 \times 10^{-14}$ cm^2 s^{-1}. In comparison, the existing literature reports diffusion co-efficients of Li in graphitic carbons between 10^{-6} and 10^{-16} cm^2 s^{-1}.[7–10,31,32] Several reasons for this wide variation have been described by Ceder et al.; (a) techniques/methods used to measure and estimate the diffusivities have been different; (b) graphitic carbons possess a wide variety of different structures; (c) the large anisotropy in the Li diffusivity parallel and perpendicular to the basal planes.[7] This work also reports an approximate value of $\approx 10^{-12}$ cm^2 s^{-1} for the average Li diffusivity perpendicular to the graphene layers. Uchida et al.[32] also experimentally measured a similar Li diffusion coefficient of $\approx 10^{-12}$ cm^2 s^{-1} during electrochemical cycling of electrodes made of well graphitized carbon fibres. These values are similar to those observed with the c-axis oriented structure of the CVD C films, where the Li-ions have to diffuse perpendicular to the (0001) basal planes.

As already noted, the larger capacity at fast C rates in the VAGLA films indicates faster transport. However, the variation of f with cycling rate for the VAGLA films does not fit the form of Equation (5) as well as the CVD data. For example, if D was an order of magnitude faster for the VAGLAs, the curve in Figure 4b would merely shift to the right to reflect the corresponding lower value of ρ. Instead, the VAGLA capacities decrease more slowly over a wider range of C rates. A plausible explanation for this discrepancy is other impedance in the system that reduces the Li transport rate at higher C rates. Here, it should be noted that the cells used for the in situ stress measurements exhibit more impedance than typical coin cells, and we have recently seen analogous kinetic limitations at similar current densities in our in situ stress work with Si films.[32,36] The well-behaved, linear decrease in capacity (on this log plot) suggests that a single mechanism dominates this impedance, such that Li diffusion in the films is likely to be fast over this range of C rates. Based on this, we believe that the Li diffusivity in the VAGLA films is at least one order of magnitude faster, and probably more than two orders of magnitude faster than the relatively slow rate in the CVD material (as tentatively inferred from Figure 4b). More precise experiments to determine D in these films are currently underway, using standard electrochemical methods.

3. Conclusion

In summary, we have demonstrated that graphenic carbon thin films with graphene layers oriented perpendicular to the substrate allow direct access for Li-ions to the graphene interlayer spaces. Such crystallographic orientation of the graphenic

lattice results in faster Li-intercalation/de-intercalation, allowing better capacity retention at higher electrochemical cycling rates, as compared to CVD carbon films where the graphene layers are parallel to the substrate. With further development of materials with vertically aligned graphene layers it should be possible to obtain higher capacities at the faster cycling rates. These electrodes also possess excellent Li-capacity and show isotropic in-plane behavior when produced by spin-coating, whereas strong anisotropic stress development occurs when the vertically aligned graphene layers are directionally oriented along the plane of the substrate via bar-coating, which flow-aligns the precursor molecular disks. Overall, we report that the orientation of the graphene layers can be engineered to create graphenic thin films with highly anisotropic properties, and that these materials can lead to carbon-based anodes for high power Li-ion batteries. Further improvement may be possible by developing VAGLA precursors based on highly condensed polyaromatic molecules with larger size and lower heteroatom content to reduce defect density within the vertically aligned graphene layers following carbonization and annealing.

4. Experimental Details

VAGLA films were obtained by coating 250-µm-thick (1-inch diameter) quartz wafers with aqueous solutions of optimized concentrations (based on I-N phase transitions[13,37]) of chromonic liquid crystal (CLC) precursors (obtained from Optiva, South San Francisco, CA). Prior to the coating, 15-nm-thick Ti adhesion interlayer, followed by 200-nm-thick Ni layer, were deposited via e-beam deposition on the quartz wafers. About 20 µL CLC precursor was applied to the substrate and spread into uniform films using either spin-coating (3000 rpm for 30 s) or using Mayer-bars (RD Specialties Inc., Webster, NY) with the winding metal wire diameter of 0.08, 0.20, and 0.51 mm, respectively (bar-coating). For graphitization, annealing was performed under an argon atmosphere at 1000 °C for 1 h. More details concerning the development of VAGLA films can be found in our previous publication.[13] Different approaches to prepare graphene based materials starting from various chemical precursors have also been reviewed by Zhi and Mullen.[38] The CVD C films were obtained by chemical vapor deposition (CVD) on the similar substrate/metallic interlayer layer combination at 1000 °C for 1 h using a mixture (1:1, v/v) of propylene gas and forming gas (95% Ar + 5% H_2) at a pressure of 10 Torr.[15,19]

The films were characterized using high resolution transmission electron microscopy (HRTEM; JEOL 2010FS). Cross-sectional samples for HRTEM were prepared following the TEM lift-out technique in a dual-beam focused ion-beam (FIB; FEI HELIOS 600). FIB was also used to look at the cross-section and determine the film thicknesses (≈200 nm).

The electrochemical behaviors of both the films were investigated during galvanostatic discharge/charge cycles against Li metal in a custom made electrochemical cell. More details about the cell and the cycling procedures can be found in our previous publications.[15,19,32,36,39] The liquid electrolyte used was an equimolar mixture of ethylene carbonate (EC) and dimethyl carbonate (DMC) containing 1 M LiPF6 salt. The cell was subjected to galvanostatic cycles (at constant currents) between 2 and 0.001 V, using different electrochemical cycling rates (from C/20 to 10C). The back surface of the substrate was visible through a transparent quartz window on top of the sealed cell, which made it possible to monitor bending of the thin film specimen using the MOSS. By monitoring the changes in the spot spacing (deflections) of laser beams reflected from the back side of a substrate, MOSS is used for real time (in situ) determination of the wafer (substrate) curvature induced by stress development in thin films.[15–17,32,36,39] This allowed us to monitor the stress development parallel to the current collector in the CVD C thin film electrodes, in situ during the electrochemical cycling. Since only the initial film thicknesses are known, the reported stress data are quoted as "nominal stress"[15,19,36,39] (σ^{NOM} = stress-thickness[15,17–19,32,36,39]/initial film thickness).

Acknowledgements

The authors would like to acknowledge Dr. M. P. Gururajan, IIT Bombay, India, for assistances with some of the curve fittings. This work was supported by NSF, under awards CMMI-1000822, DMR-0805172, and DMR-0520651 (MRSEC), by the GM/Brown CRL on Computational Materials Science, by the Korea Institute of Machinery and Materials, and by KIST. We are also grateful to Dr. Pavel Lazarev of Ribtan Inc. for sample donations.

Received: April 23, 2012
Revised: November 12, 2012
Published online: January 6, 2013

[1] J. M. Tarascon, M. Armand, *Nature* **2001**, *414*, 359.
[2] Y. Wang, G. Cao, *Adv. Mater.* **2008**, *20*, 2251.
[3] M. Wakihara, *Mater. Sci. Eng. R* **2001**, *33*, 109.
[4] B. Kang, G. Ceder, *Nature* **2009**, *458*, 190.
[5] K. Kang, Y. S. Meng, J. Breger, C. P. Grey, G. Ceder, *Science* **2006**, *311*, 977.
[6] A. D. Pasquier, I. Plitz, S. Menocal, G. Amatucci, *J. Power Sources* **2003**, *115*, 171.
[7] K. Persson, V. A. Sethuraman, L. J. Hardwick, Y. Hinuma, Y. S. Meng, A. van der Ven, V. Srinivasan, R. Kostecki, G. Ceder, *J. Phys. Chem. Lett.* **2010**, *1*, 1176.
[8] M. D. Levi, D. Aurbach, *J. Phys. Chem. B* **1997**, *101*, 4641.
[9] M. Morita, N. Nishimura, Y. Matsuda, *Electrochim. Acta* **1993**, *38*, 1721.
[10] P. Yu, B. N. Popov, J. A. Ritter, R. E. White, *J. Electrochem. Soc.* **1999**, *146*, 8.
[11] R. Baddour-Hadjean, J. Farcy, J. P. Pereira-Ramos, *J. Electrochem. Soc.* **1996**, *143*, 2083.
[12] M. Liang, L. Zhi, *J. Mater. Chem.* **2009**, *19*, 5871.
[13] F. Guo, A. Mukhopadhyay, B. W. Sheldon, R. H. Hurt, *Adv. Mater.* **2011**, *23*, 508.
[14] F. Guo, A. Mukhopadhyay, B. W. Sheldon, R. H. Hurt, *InterNano: Resources for Manufacturing,* **2011**, www.internano.org/content/view/491/239//?utm_source=newsletter&utm_medium=email&utm_campaign=nmw20110216 (accessed November 2012).
[15] A. Mukhopadhyay, A. Tokranov, K. Sena, X. Xiao, B. W. Sheldon, *Carbon* **2011**, *49*, 2742.
[16] H. Marsh, A. P. Warburton, *J. App. Chem.* **1970**, *20*, 133.
[17] E. Chason, B. W. Sheldon, *Surf. Eng.* **2003**, *19*, 387.
[18] L. B. Freund, S. Suresh, in *Thin Film Materials* (Cambridge Univ. Press, Cambridge, **2003**).
[19] A. Mukhopadhyay, A. Tokranov, X. Xiao, B. W. Sheldon, *Electrochim. Acta* **2012**, *66*, 28.
[20] E. Buiel, J. R. Dahn, *Electrochim. Acta* **1999**, *45*, 121.
[21] J. R. Dahn, T. Zheng, Y. Liu, J. S. Xue, *Science* **1995**, *270*, 590.
[22] E. Peled, D. Golodnitsky, A. Ulus, V. Yufit, *Electrochim. Acta* **2004**, *50*, 391.
[23] P. Novak, F. Joho, M. Lanz, B. Rykart, J. C. Panitz, D. Alliata, R. Kotz, O. Haas, *J. Power Sources* **2001**, *97–98*, 39.
[24] S. Zhang, M. S. Ding, K. Xu, J. Allen, T. R. Jow, *Electrochem. Solid-State Lett.* **2001**, *4*, A206.

[25] H. Buqa, A. Würsig, J. Vetter, M. E. Spahr, F. Krumeich, P. Novák, *J. Power Sources* **2006**, *153*, 385.
[26] R. Yazami, *Electrochim. Acta* **1999**, *45*, 87.
[27] J. O. Besenhard, M. Winter, J. Yang, W. Biberacher, *J. Power Sources* **1995**, *54*, 228.
[28] Y. Qi, H. Guo, L. G. Hector, A. Timmons, *J. Electrochem. Soc.* **2010**, *157*, A558.
[29] D. Billaud, E. McRae, A. Herold, *Mater. Res. Bull.* **1979**, *14*, 857.
[30] S. Yang, X. Feng, L. Zhi, Q. Cao, J. Maier, K. Müllen, *Adv. Mater.* **2010**, *22*, 838.
[31] T. Uchida, Y. Morikawa, H. Ikuta, M. Wakihara, *J. Electrochem. Soc.* **1996**, *143*, 2606.
[32] S. K. Soni, B. W. Sheldon, X. Xiao, A. F. Bower, M. W. Verbrugge, *J. Electrochem. Soc.* **2012**, *159*, A1520.
[33] A. K. Dutta, *Phys. Rev.* **1953**, *90*, 187.
[34] W. Primak, L. H. Fuchs, *Phys. Rev.* **1954**, *95*, 22.
[35] J. Crank, in *The Mathematics of Diffusion* Oxford Univ. Press, Oxford **2004**.
[36] S. K. Soni, B. W. Sheldon, X. Xiao, A. Tokranov, *Scr. Mater.* **2011**, *64*, 307.
[37] L. Onsager, *Ann. N. Y. Acad. Sci.* **1949**, *51*, 627.
[38] L. Zhi, K. Mullen, *J. Mater. Chem.* **2008**, *18*, 1472.
[39] B. W. Sheldon, A. Rajamani, A. Bhandari, E. Chason, S. K. Hong, R. Beresford, *J. App. Phys.* **2005**, *98*, 043509.